A SIMPLE MODEL TO PREDICT WEB-TO-ROLLER TRACTION

by

B. S. Rice[1] and R. F. Gans[2]
Eastman Kodak Company[1]
University of Rochester[2]
USA

ABSTRACT

We have studied the traction developed between a thin, flexible web and a rotating cylindrical roller. We present a new analytic model for high-wrap, circumferentially grooved rollers that couples air film pressure, web deflection, and asperity contact to predict traction. Our model predicts the "steady state" (far from the ends of the lubrication region) air pressure between the web and roller by judicious use of the foil-bearing concept. We verified our new model experimentally for non-grooved and high-wrap, circumferentially grooved roller surfaces. We have derived dimensionless groups that the roller designer can use to quantitatively assess the interactions of process variables (e.g., speed and tension) with design variables (e.g., groove depth, groove pitch, roughness, etc.). We also give a dimensionless group that quantifies the term *high wrap*.

NOMENCLATURE

Greek:

α	combined asperity engagement height
α_r	roller asperity engagement height
α_w	web asperity engagement height
δ	function used in defining web roller spacing without air entrainment
ΔT	T_{high0}-T_{low0}
θ	roller wrap angle
θ^*	dimensionless group that defines high wrap
μ	air viscosity
ν	web Poisson's ratio
ρ	mass density of the web

Roman:

A_{xc}	cross-sectional area
B^*	dimensionless group that defines thin web
c	web thickness
D	flexural rigidity of the web
E	Young's modulus of elasticity for web
f	static coefficient of friction
f_e	effective coefficient of friction
G_D	groove depth
G_{Deff}	effective groove depth
G_w	groove width
h	web-to-roller clearance
h_{eff}	effective web-to-roller clearance during contact
h^*	dimensionless group relating actual web-to-roller clearance to effective web-to-roller clearance
l	width of arbitrary cross-section
L_F	land fraction
L_w	land width
N	number of grooves per meter
p	air pressure under web
P_a	steady-state air pressure under the web
P_c	contact pressure between web and roller
P^*	dimensionless group relating air pressure to web tension pressure
Q	volumetric flow rate
R	roller radius
R_{pm}	surface roughness parameter, average of the five highest peaks in the sample, measured from the mean plane
R_z	surface roughness parameter, difference between the average of the five highest peaks and the five lowest valleys in the sample, measured from the mean plane
T	web tension per unit width, $T = T_0 - c\rho V_w^2$
T_0	nominal web tension per unit width
T_{high}	high-side web tension per unit width, $T_{high} = T_{high0} - c\rho V_w^2$
T_{high0}	nominal high-side web tension per unit width
T_{low}	lowside web tension per unit width, $T_{low} = T_{low0} - c\rho V_w^2$
T_{low0}	nominal lowside web tension per unit width
$u(y,z)$	velocity profile over arbitrary cross-section
V	transport velocity, $V = V_r + V_w$
V_r	roller transport velocity
V_w	web-transport velocity
w	web displacement
x	longitudinal spatial coordinate
y	cross-width spatial coordinate
z	spatial coordinate perpendicular to web

INTRODUCTION

We have analytically and experimentally studied the traction developed between a thin, moving flexible web wrapped around a rotating cylindrical roller with circumferential grooves. In most applications, web-to-roller traction is the key to successful use of rollers. The maximum average contact pressure between the web and roller is at zero speed. As the web and roller speed increase from zero, the converging geometry of the inlet region of the web/roller interface acts as a wedge bearing, resulting in super-ambient air pressure between the web and roller. The magnitude of the super-ambient air pressure increases with speed, causing a corresponding decrease in contact pressure. Eventually, further increases in speed will cause the average air pressure between the web and roller to exactly balance the pull down pressure, *T/R*, causing complete lack of contact. Any further increase in speed only increases the spacing (flying height) between the web and roller.

The tension differential that a cylindrical roller can support in the absence of air lubrication is a function of the static coefficient of friction *(f)*, wrap angle *(θ)*, and the normal pressure between the web and roller. In the absence of lubrication, the well-known band brake or capstan equation can be used to estimate the maximum web tension differential that can exist across a roller. At impending slip, the following equality is satisfied:

$$\frac{T_{high}}{T_{low}} = e^{f\theta}, \qquad \{1\}$$

where $T_{high} = T_{high0} - c\rho V_w^2$, $T_{low} = T_{low0} - c\rho V_w^2$, T_{high0} denotes the high-side web tension per unit width, T_{low0} denotes the low-side web tension per unit width, c denotes the web thickness, ρ denotes the web mass per unit volume, and V_w denotes the web speed.

Daly [1] was the first to observe that the capstan equation predictions of web-to-roller traction were invalid as a result of air entrainment. The first "predictive" capabilities of web-to-roller traction were by Knox and Sweeny [2] in 1971. Today, modeling web-to-roller traction has evolved to finite difference (FD) fluid/structure interaction codes [3, 4, 5], but the roller designer is left with a difficult task. The investment of time and education needed to implement these codes is large. In addition, these codes require considerable computer resources. Depending on the size of the mesh required, a 2D fluid structure interaction code may take from several hours to several weeks to run on today's computers (2 GHz processing speed). Therefore, the roller designer typically resorts to trial-and-error experimental techniques to design a roller with adequate traction.

Roller and web surface roughness, roller relief feature characteristics (e.g., groove depth, width, and pitch), tension, and speed are common design variables investigated experimentally. A standard technique to measure how well a roller reduces the effects of air entrainment is to measure the maximum tension differential a roller can support at a specified small percentage of slip [2,3,5,6,7]. This can be done in the actual machine or in an off-line test facility. These experimental measurements are presented in two general ways. The first method is to simply state the maximum tension differential: $\Delta T = T_{high0} - T_{low0}$. The second and more common method is to report traction in terms of the effective coefficient (f_e), which is computed as follows [5]:

$$f_e = \frac{1}{\theta}\ln\left[\frac{T_{high0}}{T_{high0} - \Delta T}\right]. \qquad \{2\}$$

Eq. 2 is simply the capstan equation where f_e has replaced f, the centripetal acceleration ($-c\rho V_w^2$) term has been neglected, and T_{low0} has been replaced by T_{high0}-ΔT. The effects of air lubrication and centripetal acceleration are commonly lumped together. At very low speeds, f_e is approximately equal to the static coefficient of friction f. As speed increases, f_e decreases as a result of air entrainment. Typically, the roller designer desires a certain value for f_e. Using trial-and-error techniques, the required groove depth and surface roughness are eventually found that yield the desired result.

This trial-and-error experimental technique is both costly and time consuming. We seek to identify and isolate the important parameters determining traction. Our goal is a simple model that can be used to design rollers with adequate traction for the desired operating conditions. To this end, we again derive the capstan equation for non-grooved or high-wrap circumferentially grooved rollers in the presence of air lubrication, including centripetal acceleration.

Web and roller surfaces are unavoidably rough; therefore, the contact is dominated by asperity contact. We suppose that traction will be good if the asperity contact forces between the web and roller are much greater than the unavoidable air pressure forces caused by the lubrication layer for a significant part of the nominal contact region. This paper is devoted to the quantification of this idea. We address the "steady-state" air pressure far from the entrance region by judicious use of the foil bearing concept, adapting the foil bearing equation to the case of non-grooved and high-wrap circumferentially grooved rollers using basic physical principles.

We introduce the concept of an effective web-to-roller clearance (h_{eff}). For non-grooved rollers, we use the model of Rice *et al.* [5], which determines h_{eff} based on the surface roughness parameters R_{pm} and R_z of both surfaces. The effective web-to-roller clearance allows us to map two rough surfaces in contact to two equivalent smooth surfaces not in contact. The effective web-to-roller clearance accounts for the increased flow resistance due to roughness.

Grooves provide an additional channel for air to flow during contact. The effective web-to-roller clearance associated with the grooves is the spacing between two parallel plates that has the same average volumetric flow rate as the real grooved roller has during contact, given the same pressure gradient. Again, we address the steady-state air pressure far from the entrance region by judicious use of the foil bearing concept, adapting the foil bearing equation to the case of a grooved roller with contact using basic physical principles.

ANALYTICAL TRACTION MODEL

Web/Roller System

A schematic of a web roller system with the appropriate coordinate system is shown in Fig. 1. Web deflection is in the z direction and is labeled w. The parameter δ is a function of x and y and represents the web-to-roller spacing without air entrainment. The air gap h is equal to $w+\delta$. Later in the paper, we will exploit the symmetry boundaries shown in Fig. 1 in the development of a simple traction model for grooved rollers.

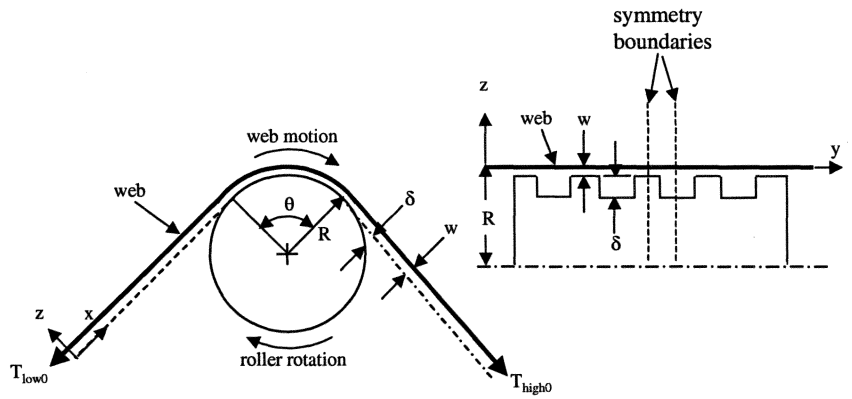

Fig. 1. Roller/web schematic and coordinate system.

Foil Bearing Equation Used to Predict Air Pressure

The foil bearing equation was derived based on the assumptions of a 1D Reynolds equation, incompressible fluid, constant web tension, no web bending stiffness, no contact between the web and roller, and perfectly smooth web and roller surfaces. Eshel and Elrod [8] found the solution to the foil bearing problem using matched asymptotics. The problem has three regions: (1) entrance, (2) constant gap and pressure, and (3) exit. Fig. 2 shows the web-to-roller gap and the air pressure in these three regions. The pressure smoothly rises above ambient as a result of the converging geometry of the entrance region. The pressure in the center region is constant and equal to the pressure due to web tension, *T/R*. In the exit region, the pressure drops below ambient because of the diverging geometry of the exit region.

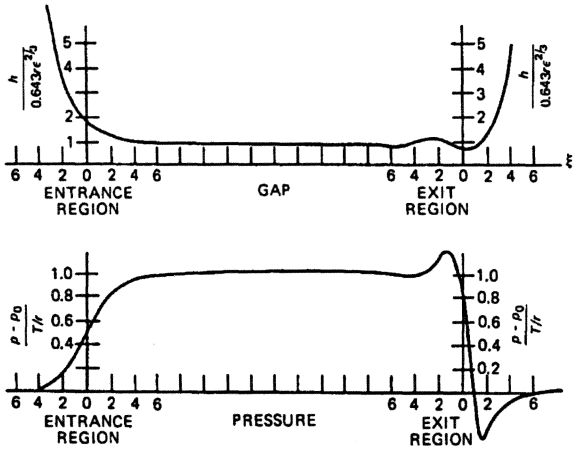

Fig. 2. Foil bearing gap and pressure profile (reproduced from Gross [18])

The foil bearing equation [8] gives the fluid gap h in the center region:

$$h = 0.643R\left[\frac{6\mu V}{T}\right]^{2/3}, \qquad \{3\}$$

where R denotes the roller radius, μ the dynamic viscosity of air, $V = V_r + V_w$, where V_r denotes the roller surface speed and V_w the web speed. Knox and Sweeny [2] and Ducotey and Good [6] have used the foil bearing equation with varying degrees of success to provide qualitative data explaining web-to-roller traction for non-grooved rollers.

Normally, the foil bearing equation is used to compute the gap h based on a given R, T, V, and μ. We rewrite it as a predictor of P_a:

$$P_a = \frac{3.094 \mu V}{R} \left(\frac{R}{h} \right)^{3/2} . \qquad \{4\}$$

In the roller traction problem, two of the assumptions used in the foil bearing derivation are violated: (1) we desire contact between the web and roller; and (2) real webs and rollers surfaces are rough. To use the foil bearing to predict the constant gap/pressure region in the presence of contact, we assume that contact does not change the geometry of the entrance nip. We believe this to be reasonable based on Fig. 2, which shows the entrance nip geometry smoothly approaching the radius of the roller. The presence of contact should not affect this. The exit region is very different. As a result of the undulating nature of the exit region, the minimum clearance is 71.6 % of the nominal clearance. When contact is not desired (head/tape problem), the minimum clearance in the exit region would be of importance. In most typical roller problems, contact is desired over the entire wrap angle. Assuming we have contact in the constant gap region, web deflection further toward the roller as predicted by the foil bearing equation would be prevented by contact. Because the flow of information is from the constant gap region to the exit region, modifications to the exit region's shape only have local implications. The large constant gap region remains unchanged. The constant clearance region is large compared to the entrance and exit regions for moderate to large wrap angles; so the effects of the entrance and exit regions can be ignored.

Let us model the roller surface roughness by infinitesimally thin, but rigid, supports supposed far enough apart and thin enough that the airflow is not disturbed. Such supports will contact the web if their height h exceeds the spacing predicted by the foil bearing. In this case, Eq. 4 can be solved for P_a. The corresponding tension will be equal to $P_a R$, based on equilibrium considerations. This tension will produce essentially zero contact force between the web and roller. If the tension increases beyond this initial value, the air gap and, thus, the air pressure will remain the same because the web is (partially) supported by the roughness. Any increase in T beyond what is required to balance air pressure will create contact pressure, P_c, between the web and roller. The contact pressure between the web and roller, which determines the web-to-roller traction, is given by: $P_c = T / R - P_a$. (We assumed that the area over which contact pressure and air pressure act is the same. If the contact area were only half the total area, the contact pressure would be twice as high but the total force would remain the same. Because we are neglecting the deflection of the asperities, the choice of contact area is irrelevant.)

The foil bearing equation does not include the effect of surface roughness on the flow. Any real surface has roughness. As noted in the introduction, real web/roller systems can be characterized by an effective web-to-roller clearance (h_{eff}). We will generalize the expression given in [5] to include the effects of grooves in the next section. When applying the foil bearing equation to a real web/roller problem, h_{eff} plays the same role h does in the idealized foil bearing equation.

Rice *et al.* [5] showed that deformation of the asperities for typical web tensions (175 N/m) is not important in the typical web-to-roller traction problem. The assumption of infinitely stiff asperities greatly simplifies the problem because the coupling between air pressure, web tension, and asperity deflection is avoided. Substituting h_{eff} for h in Eq. 4 yields an inverted contact foil bearing equation:

$$P_a = \frac{3.094\mu V}{R}\left(\frac{R}{h_{eff}}\right)^{3/2}. \qquad \{5\}$$

Eq. 5 is only valid in the presence of contact. Clearly, a web/roller system with tall protruding asperities and/or deep grooves (large h_{eff}) is less susceptible to traction loss. The greater the effective spacing, the lower the resulting air pressure will be and the greater the contact pressure.

Effective Web-to-Roller Clearance

Rice *et al.* [5] derived an experimentally based model for the *asperity engagement height*, which allows us to map two rough surfaces in contact to two equivalent, smooth surfaces not in contact, accounting for the increased flow resistance due to roughness. We combine the web and roller heights from [5] using their *root mean square model*:

$$\alpha = \sqrt{\alpha_r^2 + \alpha_w^2}, \qquad \{6\}$$

where α_r and α_w denote the roller and web individual asperity engagement heights. This asperity engagement height is equal to h_{eff} for ungrooved rollers.

Grooved rollers require additional analysis. Patir and Cheng [10] determined flow factors by matching volume flow with roughness to volume flow without roughness for the same maximum fluid gap and pressure gradient. They used numerical simulations to determine the flow factors. We will use a similar concept for our grooved rollers. Instead of using flow factors, we will simply calculate h_{eff}. We define h_{eff} as the spacing between two parallel plates that gives the same average volumetric flow rate as the grooved roller in contact with the web for the same pressure gradient in the x-direction. This allows us to use the effective h_{eff} directly in Eq. 5. (This approach tacitly assumes a continuous connection from the inlet and outlet nips during contact. We will see (by experimental evidence) that this is a crucial assumption and an important feature of successful rough rollers.)

An analytic solution to the volumetric flux rate for even simple cross-sections is generally not possible. We will use an approximate method to find h_{eff} for arbitrary cross sections. We neglect the extra viscous drag caused by the groove sidewalls. The pressure-driven volumetric flow between two smooth parallel flat plates is equal to [11]:

$$Q = \int_{A_{xc}} u(y,z)\,dA_{xc} = -\frac{h^3}{12\mu}\frac{dp}{dx}l, \qquad \{7\}$$

where h denotes the air gap spacing, x the longitudinal spatial coordinate, μ the dynamic viscosity, l the width of the cross-section of interest, and p the pressure.

We use Eq. 7 to calculate the volume flux of the grooved roller profile in contact with smooth plate (representing the web). We also use Eq. 7 to calculate the volume flux

between two smooth parallel flat plates. We adjust the spacing between the smooth parallel flat plates until the volume flux matches that of the grooved roller profile (in contact with a smooth plate), given the same pressure gradient. The spacing between the smooth parallel plates is h_{eff}. Two smooth parallel plates spaced apart by this distance have the same average volumetric flow rate, as does the real grooved roller/web interface for the same pressure gradient in the x-direction.

We assume that Eq. 7 applies locally. Thus, for any infinitesimal slice, dy, flow is proportional to the spacing $h(y)$ raised to the third power. Equating flow for parallel plates spaced h_{eff} apart to the volume flow of an arbitrary cross-section and solving for h_{eff} yields:

$$h_{eff} = \left[\frac{1}{l} \int_0^l h^3(y) dy \right]^{1/3}, \qquad \{8\}$$

where y is the coordinate in the cross-width direction. Rice [12] shows that Eq. 9 is extremely accurate for the groove width (G_W) to groove height (G_D) aspect ratios discussed in this paper; the error is of order $(G_D/G_W)^2$.

Important Dimensionless Groups

We have shown that contact, surface roughness, and grooves do not preclude the use of the foil bearing equation to predict the constant gap and pressure region. This suggests that using the inverted foil bearing equation to design roller surface relief features is valid. We will verify this experimentally later in this paper.

An important dimensionless group in the web-to-roller traction problem, h^*, denotes the ratio of the height predicted by the foil bearing equation to h_{eff}:

$$h^* = \frac{h}{h_{eff}} = \frac{0.643R\left[\frac{6\mu V}{T}\right]^{2/3}}{h_{eff}}. \qquad \{9\}$$

When h^* is equal to or greater than unity, the traction between the web and roller is assumed to be equal zero because the tallest features are no longer tall enough to protrude through the air film gap predicted by the foil bearing equation. When h^* is equal to zero, there is no air entrainment and full traction is realized.

Another important dimensionless group is P^*, the ratio of steady-state air pressure to the web tension pressure:

$$P^* = \frac{P_a}{T/R} = \frac{3.094\mu V}{T_0 - c\rho V_w^2}\left(\frac{R}{h_{eff}}\right)^{3/2}. \qquad \{10\}$$

When P^* is equal to or greater than unity, all the web tension pressure is balancing air pressure—$P_a = T/R$. When this happens, the web begins to float away from the roller surface and contact is lost. When P^* is equal to zero, there is no air entrainment and full traction is realized. Equation 5 is not valid when contact is lost. Using Eq. 10, Eq. 5 is modified as follows to account for loss of contact:

$$P_a = \frac{3.094\mu V}{R}\left(\frac{R}{h_{eff}}\right)^{3/2} \qquad \text{when } P^* < 1$$
$$P_a = T/R \qquad \text{when } P^* \geq 1 \qquad . \qquad \{11\}$$

Modified Capstan Equation

In the roller traction problem, we want to determine the maximum tension differential that a roller can support in the presence of air lubrication. To this end, we will derive a modified capstan equation taking into account air lubrication and centripetal acceleration. (In a similar analysis, Jones [13] reduces the inlet and outlet tensions used in the capstan equation in proportion to the calculated air pressure between the web and roller. In determining the air pressure, he incorrectly assumed that the web went from perfectly flat to the radius of the roller, similar to the Blox and vanRossum's [14] foil bearing analysis. In our derivation, we instead assume that Eq. 11 gives the air pressure.)

We suppose that web tension is uniform in the cross-width (y) direction, the system is infinitely wide (neglect edge effects), the fluid is incompressible, the web is a membrane in the circumferential (x) direction and rigid in the cross-width (y) direction, that airflow is possible during web-to-roller contact through the voids in the mating surfaces, that there is continuous connection from the inlet and outlet nips during contact, that contact and air pressure act over the same area ($R\theta W$), and that the asperities are infinitely stiff.

Figure 3 shows a free-body diagram of an infinitesimal portion of web shown in Fig. 1 at impending slippage. Two normal forces are present, dN_c (due to contact) and dN_a (due to air pressure). Two frictional forces are also present fdN_c (due to contact) and F_{air} (due to air viscous forces). Ducotey and Good [6] showed that F_{air} is small and of no practical importance to the roller traction problem, and we neglect it from here onward.

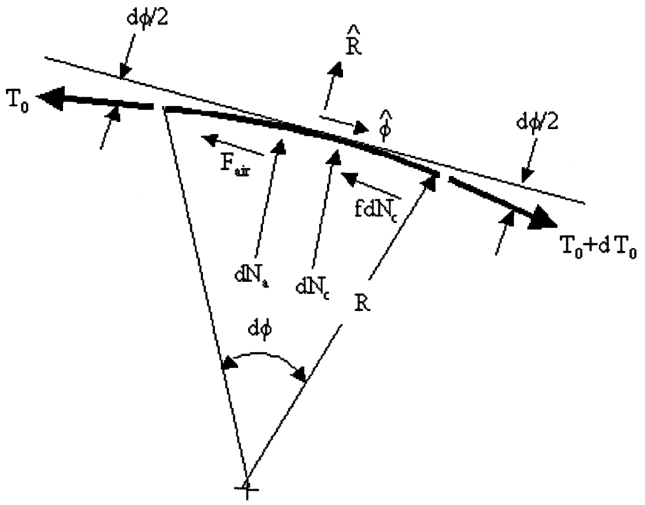

Fig. 3. – Free-body diagram of an infinitesimal portion of web at impending slippage.

We assume that the air pressure (given by Eq. 11) is uniform in the contact zone, that f is independent of load, and that there is impending slippage between the web and roller.

Summing forces in the radial and circumferential directions, making the usual small angle approximations, eliminating dN_c, and integrating over the contact region yields the modified capstan equation:

$$\frac{T_{high} - P_a R}{T_{low} - P_a R} = e^{f\theta}, \qquad \{12\}$$

where P_a is given by Eq. 11.

Equation 12 is the capstan equation including the effects of air entrainment and centripetal acceleration for non-grooved and high-wrap circumferentially grooved rollers at impending slippage. This is an extremely simple equation that can be used to predict how traction is affected by air entrainment. Solving for T_{high}-T_{low} in Eq. 12 yields the web-to-roller traction (ΔT) when T_{high} is held fixed in the presence of an air lubricating film:

$$\Delta T = T_{high} - T_{low} = (T_{high} - P_a R)\frac{(e^{f\theta} - 1)}{e^{f\theta}}. \qquad \{13\}$$

Similarly when T_{low} is held fixed:

$$\Delta T = T_{high} - T_{low} = (T_{low} - P_a R)(e^{f\theta} - 1). \qquad \{14\}$$

EXPERIMENTAL TRACTION MEASUREMENTS AND RESULTS

The test facility used in this paper is described in detail in [5] and [12]. The equivalent coefficient of friction is measured by applying a slowly increasing braking torque using a pneumatically actuated PRONY brake [15] to the test roller until slip is detected between the test roller and web. Slip is supposed to have occurred when the ratio of the time required for one revolution of the test roller to the time required for one revolution of a reference roller varies by more than 0.3 % from a reference value.

Substitution of our new 1D model, Eq. 14 into Eq. 2 yields:

$$f_e = \frac{1}{\theta}\ln\left[\frac{T_{high0}}{T_{high0} - \left[(T_{high} - P_a R)\frac{(e^{f\theta} - 1)}{e^{f\theta}}\right]}\right], \qquad \{15\}$$

where P_a is given by Eq. 11. This equation allows us to compare our modified capstan equation directly to experimental roller traction data.

Description of all the webs and rollers used for experiments in this paper are given in Tables 1 and 2, respectively. The appropriate values for: h_{eff}, f, θ, α, T_{high0}, etc., needed for the 1D model are given in Table 3. The static coefficient of friction is estimated from the y intercepts of the plots of effective coefficient of friction versus speed [12]. We measured the surface roughness parameters for the webs and roller with an optical surface profiler using techniques described in Rice [12].

web #	description	thickness (μm)	density (kg/m^3)	Young's Modulus (Pa)	R_{pm} mean (μm)	R_{pm} std (μm)	R_z mean (μm)	R_z std (μm)	α_w (μm)
1	PE coated paper	272	1108	4.14E+09	6.08	0.62	10.88	0.60	8.76
2	coated PET	182	1358	4.83E+09	4.99	0.62	5.74	0.66	5.64
3	coated PET	179	1358	4.83E+09	1.04	0.14	1.22	0.20	1.19
4	uncoated PET	98	1358	4.83E+09	0.61	0.30	0.72	0.32	0.71
5	coated PET	180	1358	4.83E+09	1.45	0.17	1.55	0.14	1.54
7	coated PET	100	1358	4.83E+09	0.57	0.19	0.68	0.21	0.66
8	coated PET	125	1358	4.83E+09	0.76	0.04	1.39	0.03	1.11
17	coated PET	125	1358	4.83E+09	2.16	0.42	2.41	0.47	2.38
18	coated PET	125	1358	4.83E+09	0.60	0.08	0.79	0.12	0.74

Webs 1-4 were 0.7 m wide. All other webs were 1.4 m wide, except web 8 was 0.7 m wide for the 350 N/m test only.

Table 1. Web description.

roller #	surface material	radius (m)	N (m^{-1})	G_D mean (μm)	G_D std (μm)	tool radius (μm)	L_F	R_{pm} mean (μm)	R_{pm} std (μm)	R_z mean (μm)	R_z std (μm)	α_r (μm)
1	aluminum hardcoat	0.050	n/a	n/a	n/a	n/a	n/a	1.44	0.12	7.67	2.09	2.61
2	tungsten carbide	0.050	n/a	n/a	n/a	n/a	n/a	17.1	1.82	35.3	1.86	25.9
3	nickel plated	0.050	3937	43	4	127	0.25	1.25	0.09	2.88	0.20	1.96
4	nickel plated	0.050	3937	36	3	127	0.31	0.23	0.07	0.63	0.15	0.38
15	stainless steel	0.050	n/a	n/a	n/a	n/a	n/a	8.62	2.91	37.4	5.06	15.3

All rollers were 1.5 m wide.

All roughness measurements are for the land portion only, except rollers 1, 2, and 15 are total surface.

Rougness wasn't measured for rollers 13 and 14, typical values were used from similar rollers.

GD std for rollers 13 and 14 is based on typical values for rollers made with similar manufacturing processes.

Table 2. Roller description.

roller #	web #	θ (deg)	α (μm)	f	T_0 (N/m)	G_{Deff} (μm)	h_{eff} (μm)
1	1	90	9.1	0.35	175	n/a	9.1
1	2	90	8.3	0.20	175	n/a	8.3
1	3	90	3.8	0.20	175	n/a	3.8
1	4	90	3.3	0.20	175	n/a	3.3
2	5	90	25.9	0.55	44	n/a	25.9
2	5	90	25.9	0.55	88	n/a	25.9
2	7	90	25.9	0.35	44	n/a	25.9
2	7	90	25.9	0.35	88	n/a	25.9
15	5	90	15.3	0.25	88	n/a	15.3
15	5	90	15.3	0.25	131	n/a	15.3
15	7	90	15.3	0.25	88	n/a	15.3
15	7	90	15.3	0.25	131	n/a	15.3
3	5	90	2.5	0.49	88	n/a	29.2
3	7	90	2.1	0.43	88	n/a	29.2
4	8	88	1.1	0.16	350	27.9	24.7
4	8	10	1.1	0.13	350	27.9	24.7
4	17	84	2.4	0.21	88	27.9	24.7
4	17	84	2.4	0.26	131	27.9	24.7
4	18	84	0.7	0.26	88	27.9	24.7
4	18	84	0.7	0.29	131	27.9	24.7

μ_a =1.81e-5 N-s/m^2

p_{atm}=101e5 Pa

Table 3. Run description.

Figure 4 shows the comparison of f_e predicted by the 1D model presented in this paper, Eq. 15, with the 1D FD code predictions, and the experimental measurements of f_e from Rice *et al.* [5]. Roller 1 is a non-grooved roller. Webs 1 through 4 have very different surface roughness characteristics. The error bars on the experimental data represent 95% confidence limits of the experimental data.

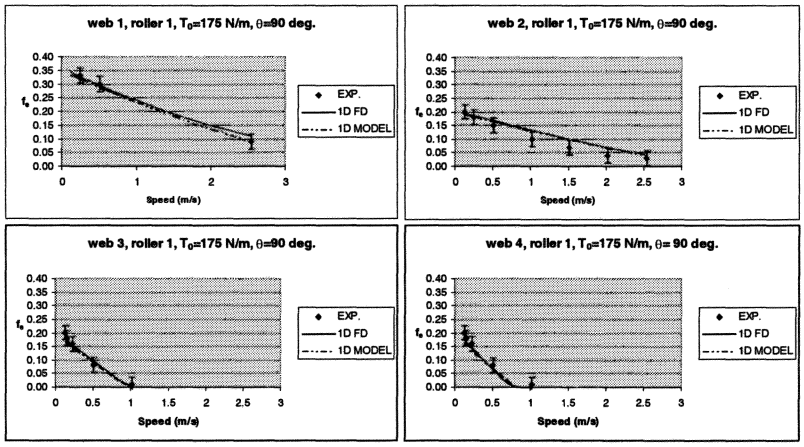

Fig. 4. Model versus experimental data and FD model from Rice *et al.* (2002).

Figure 4 shows that the 1D model based on the foil bearing, Eq. 15, agrees closely with the 1D FD code and the experimental data from Rice *et al.* [5]. Equation 15 accounts for varying tension in the circumferential direction produced by the dynamic traction tester; the 1D FD code does not. To account for the variation in tension, Rice *et al.* [5] used the average of T_{high0} and T_{low0} measured from the dynamic traction tester as the web tension in their model. Without this correction the 1D FD code would have an incorrect (too high) web tension and over-predicted traction.

Good agreement of the 1D model with 1D FD code and experimental data lends credence to our assumptions that asperity compliance and non-uniformities in air and contact pressures in the entrance and exit region can be neglected. The ability to use the 1D model instead of a 1D code greatly reduces the computational cost. In addition, greater physical insight into the web-to-roller traction problem is gained from the simple nature of our model.

We also conducted traction experiments with two additional non-grooved rollers (2 and 15) using two different webs (5 and 7). Roller 2 is manufactured using a thermal spray process, and roller 15 is manufactured using a shot-blast process [16]. Both rollers 2 and 15 have a very rough surface compared to the roller used in Rice *et al.* [5], but there is a key difference: roller 2 has its down features well-connected while roller 15 has them isolated.

Figure 5 shows plots of experimental data versus the 1D model, Eq. 15, for roller 2. Roller 2 was tested with webs 5 and 7 at two different tension levels. Roller 2 shows very good correlation between experiment and the model. The model predicts that zero traction is reached around 4.1 m/s for both webs when web tension is 44 N/m. Based on traction measurements, both webs 5 and 7 still have a minimal amount of traction at 5 m/s and 44 N/m of web tension. The difference between the experiment and model is most likely due to the undulating nature of the exit region (see Fig. 2). A small amount of contact is possible in the exit region where our model, which is based on the nominal

clearance, predicts a complete loss of contact. Because it is our desire to design rollers that have robust traction, the effects of exit region can be safely ignored.

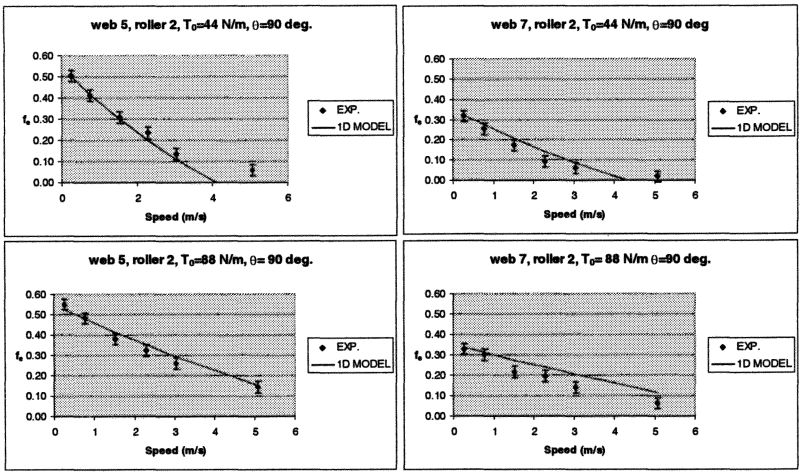

Fig. 5. Model versus experimental data for roller 2, the thermal sprayed roller.

Figure 6 shows plots of experimental data versus the 1D model for roller 15. Roller 15 was tested with webs 5 and 7 at two different tension levels. For roller 15 the correlation between experiments and the model is poor. This shot-blasted roller has large, flat-raised surfaces. The down features, where air can flow, are not well connected, as noted above. This violates one of the key assumptions required by our 1D model—a continuous connection for airflow between the inlet and outlet nips during contact. The thermal sprayed roller (2) has large round raised-up features. The down features, where air can flow, are well connected. Our new 1D model predicts traction well for cases where there is a continuous connection from the inlet nip to the outlet nip for airflow. It appears that the lack of a continuous flow path is the reason for the poor correlation of the 1D model with experiments for the shot-blasted roller (15).

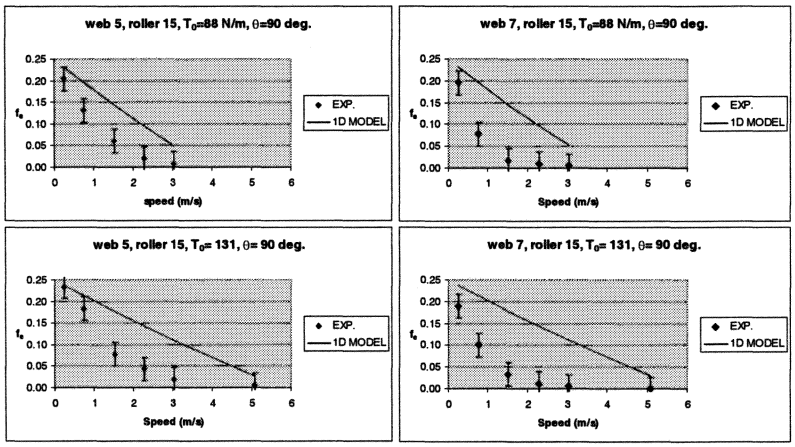

Fig. 6. Model versus experimental data for roller 15, the shot-blasted roller.

Circumferentially grooved rollers are a common method to reduce the effect of air entrainment on roller traction [17]. Figure 7 shows cross -sections of two circumferentially grooved rollers. The initial roller of interest is identified as roller 3. Roller 3 was tested using webs 5 and 7.

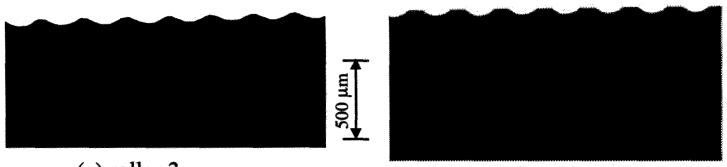

(a) roller 3 (b) roller 4

Fig. 7. Roller groove cross-sections using surface replicas: (a) roller 3; (b) roller 4.

Up to this point, we have used an optical profiler to compute h_{eff} heuristically. In this example, we will use Eq. 8 to compute h_{eff}. The surface roughness of the web and the surface roughness of the macroscopic "up features" on the roller are small compared to the groove depth (G_D) and will be ignored. In this problem, the surface is simple enough to model as a flat plate sitting on the peaks of a plate with a sine wave surface roughness, see Fig. 8. The effective height, h_{eff}, is:

$$h_{eff} = \left[\int_0^{\pi} \frac{R_z^3 \{1-\cos(y)\}^3 \, dy}{\pi} \right]^{1/3}, \qquad \{16\}$$

where the amplitude of the sine wave is equal to the G_D (43 µm), and y denotes the cross-width spatial coordinate. Note that Eq. 16 is only valid for the case where one surface is smooth and the other is a sine wave. Other groove profiles must be modeled according to the shape of their cross-section.

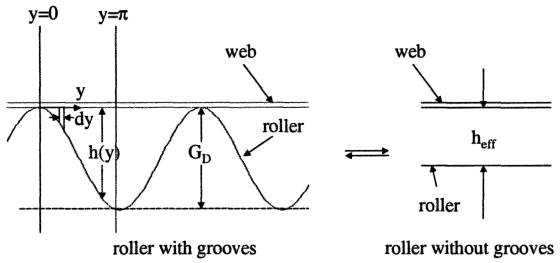

Fig. 8. Equivalent grooved roller model.

Equation 16 gives h_{eff} equal to 29.2 µm. Web tension was 88 N/m, the roller radius was 0.050 m, and the wrap angle was 90°. Table 3 shows other information required to use the 1D model. The effective coefficient of friction based on experiments, Eq. 2, and our new traction model, Eq. 15, is shown in Fig. 9 for roller 3 with webs 5 and 7. Excellent correlation between the 1D model and experimental data is seen.

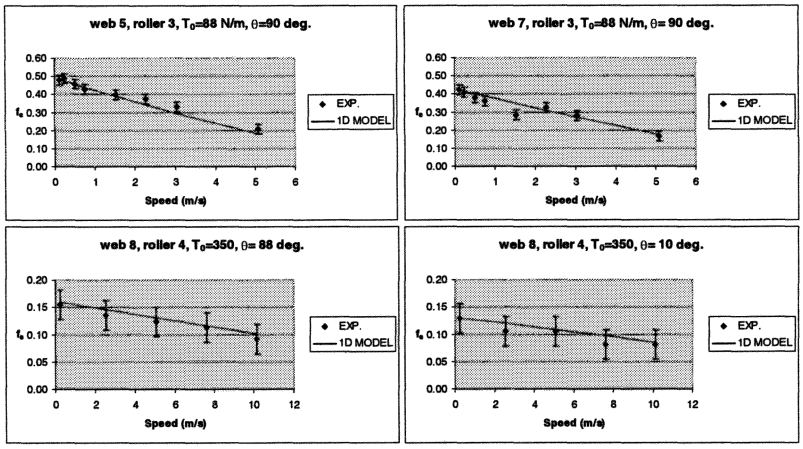

Fig. 9. Model versus experimental data using flow-based model for h_{eff}.

Figure 7 also shows a cross-section of roller 4. For this case, we'll assume there is only flow in the grooves. As in the previous example, we assume that Eq. 7 applies locally. Equation 8 still applies if h_{eff} is replaced by with the effective groove depth (G_{Deff}) for this example. The effective groove depth represents the equivalent, rectangular-shaped groove that was the same volume flow as the curved-shaped groove. This is depicted schematically in Fig. 10. The effective groove depth is calculated as follows:

$$G_{Deff} = \left[\frac{1}{G_W} \int_{-G_w/2}^{G_w/2} h^3(y)dy \right]^{1/3} , \qquad \{17\}$$

where G_w denotes the groove width and y denotes the cross-width spatial coordinate.

The groove profile is well represented as a segment of a circle. The radius of the circular segment (the manufacturing tool radius) will be referred to as r_{tool}. Thus, G_{Deff} can be calculated using the following equation (see Fig. 10):

$$G_{Deff} = \left[\frac{1}{G_W} \int_{-G_w/2}^{G_w/2} \left\{ \sqrt{r_{tool}^2 - y^2} - r_{tool} + G_D \right\}^3 dy \right]^{1/3} . \qquad \{18\}$$

The groove depth, groove width, and tool radius, for roller 4 are 36, 175.3, and 127 μm, respectively. Equation 18 gives G_{Deff} equal to 27.9 μm. This represents the effective depth of the groove. The effective web-to-roller clearance is less than the effective groove depth because airflow only occurs in the grooves.

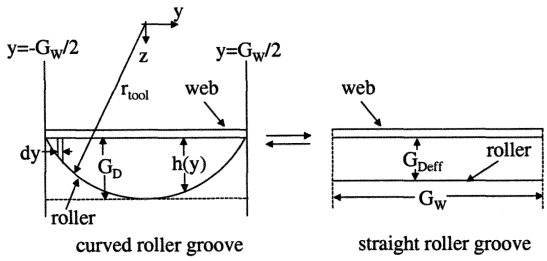

Fig. 10. Equivalent groove depth of a curved-roller groove.

The flow in the grooves will be modeled as the flow between two parallel flat plates spaced the G_{Deff} apart. Due to symmetry only, a single land and single groove needs to be considered. The spacing between two flat plates, h_{eff}, that yields the same volumetric flow as the actual roller cross-section given the same pressure gradient is calculated as follows:

$$h_{eff} = G_{Deff}\left[\frac{G_w}{G_w + L_w}\right]^{1/3}, \qquad \{19\}$$

where G_{Deff} denotes groove depth calculated by Eq. 18, G_W denotes the groove width, and L_W denotes the land width.

Equation 19 gives h_{eff} equal to 24.7 μm for roller 4. Again, roller and web asperity roughness is small compared to G_D and will be ignored. The effective coefficient of friction for roller 4 from experiments, Eq. 2, is compared to our new 1D model, Eq. 15, in Fig. 9. Web tension was 350 N/m, roller radius was 0.0508 m, and the wrap angle was 88° and 10°. Once again, good correlation between the model and experimental data is seen.

Two additional webs, 17 and 18, were tested against roller 4 at two tension levels to further verify the model. Figure 11 shows the results. Once again, correlation between model and test was excellent.

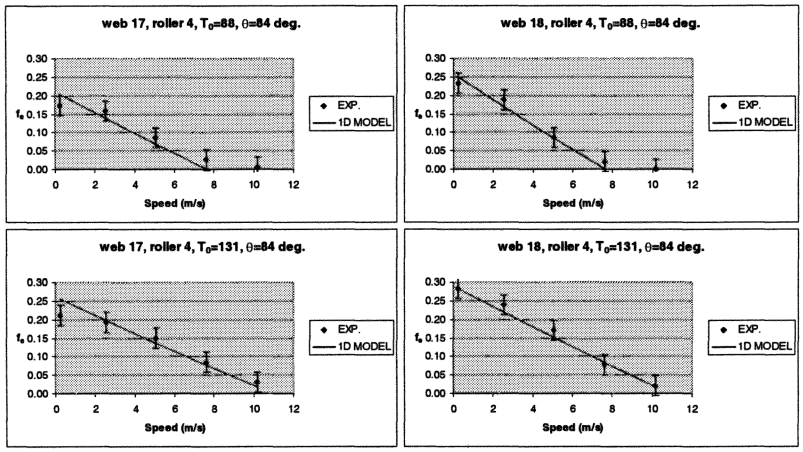

Fig. 11. Model versus experimental data for 3937 grooves-per-meter rollers.

LIMITING CONDITIONS ON THE 1D MODEL

Equation 11 is only valid in the constant pressure region of the wrap angle (see Fig. 2). Rice [12] shows that the presence of grooves reduces this constant pressure region. The 1D model is valid when the ratio of the time to reach steady state to the time the web is wrapped around the roller is small (i.e., less than 10%); this will be termed *high wrap*. Rice [12] uses a squeeze film analysis to determine this constraint (θ^*):

$$\theta^* = \frac{1}{2R\theta \cdot \alpha^2} \cdot \frac{\mu \cdot L_W^2 \cdot L_F \cdot V_w}{T/R - P_a} < 0.1, \qquad \{20\}$$

where $L_F = \frac{L_W}{L_W + G_W}$. When this constraint is violated, there is inadequate time (wrap angle) to squeeze air off the lands into the grooves.

None of the experiments reported above violate the constraint given by Eq. 20. However, when coarse pitch grooves and/or small wrap angles are used, this constraint can be violated. For coarse pitch groove patterns, the distance the air must travel on the lands to get into the grooves is large. For a roller with a low wrap angle, the time on the roller is shorter—meaning there is less time for the air to bleed into the grooves and poor traction results. The 1D model was valid with wrap angles as low as 10° because the roller grooves had a fine pitch—$\theta^* \sim 0$. This would not be true for a roller with coarse pitch grooves.

Another important assumption is that the web is rigid in the cross-width (y) direction. *What defines rigid?* When the ratio of the web deflection (w) to the web thickness (c) is small (i.e., less than 10%). Rice [12] derives this constraint (B^*):

$$B^* = \frac{(T/R)(1/N)^4}{cD} < 38.4, \qquad \{21\}$$

where $D = \frac{Ec^3}{12(1-\nu^2)}$.

None of the experiments reported above violate this constraint. When ultra-thin webs and/or when coarse-pitch grooved rollers are used, this constraint can be violated. If this happens, web deformations in the cross-width direction become significant and disrupt the airflow.

SUMMARY

The traction developed between a thin, moving flexible web wrapped around a rotating cylindrical roller with circumferential grooves was analytically and experimentally studied in this paper. In most applications, web-to-roller traction is the key to successful use of rollers.

We have developed a *modified capstan equation* that includes the effect of air entrainment for both non-grooved and high wrap circumferentially grooved rollers:

$$\frac{T_{high} - P_a R}{T_{low} - P_a R} = e^{f\theta} \quad . \qquad \{22\}$$

The term $P_a R$ represents a reduction in contact force as a result of air entrainment. An equation based on the simple foil bearing equation was derived to calculate P_a. The utility of the modified capstan equation is based on its simplicity. This equation should have broad applications in many research disciplines. Examples include: wear of the head/tape interface, torque capacity of thin belts, etc.

The modified capstan equation was verified over a wide range of process and design variables. The correlation between the model and experimental data is excellent. We showed that the modified capstan equation breaks down for roller surfaces that do not have a continuous flow path from the inlet to the outlet nips, for "low-wrap" rollers, and for "thin" webs. The dimensionless variable θ^* allowed us to quantify low warp. The dimensionless variable B^* allowed us to quantify thin webs.

The dimensionless group P^* was derived to help the roller designer easily visualize the interactions of process variables (e.g., speed and tension) with design variables (e.g., groove depth, groove pitch, etc.):

$$P^* = \frac{P_a}{T/R} = \frac{3.094 \mu V}{T_0 - c\rho V_w^2} \left(\frac{R}{h_{eff}} \right)^{3/2} , \qquad \{23\}$$

A value of P* greater than 1 means no traction and a value of 0 means no air entrainment. Now, when roller designers ask: What groove depth, groove pitch, and surface roughness are required to design a cost effective roller for a given set of process conditions?, they no longer need resort to a lengthy trial-and-error experimental approach to answer this question. The roller designer can quickly and accurately answer this question using sound engineering principles as presented in this paper.

REFERENCES

1. Daly, D. A., 1965, "Factors Controlling Traction Between Webs and Their Carrying Rolls," *Tappi Journal*, 48:9, pp. 88–90.
2. Knox, K. L., Sweeney, T. L., 1971, "Fluid Effects Associated with Web Handling," *Ind. Eng. Chem. Process Des. Develop.*, 10:2, pp. 201–205.
3. Ducotey, K. S., Good, J. K., 2000, "A Numerical Algorithm for Determining the Traction Between a Web and a Circumferentially Grooved Roller," *Trans. ASME, J. Tribology*, 122, pp. 578–584.
4. Müftü, S., Altan, M. C., 2000, "Mechanics of a Porous Web Moving Over a Cylindrical Guide," *Trans. ASME, J. Tribology*, 122, pp. 418–426.
5. Rice, B. S., Müftü, S., Cole, K. A., 2002, "A Model for Determining the Asperity Engagement Height In Relation to Web Traction over Non-vented Rollers," *Trans. ASME, J. Tribology*, Vol. 124, pp. 584–594.
6. Ducotey, K. S., Good, J. K., 1995, "The Importance of Traction in Web Handling," *Trans. ASME, J. Tribology*, 117, pp. 679–684.
7. Ducotey, K. S., Good, J. K., 1999, "Predicting Traction in Web Handling," *Trans. ASME, J. Tribology*, 121, pp. 1–7.
8. Eshel, A., Elrod, H. G. Jr., 1965, "The Theory of the Infinitely Wide, Perfectly Flexible, Self-Acting Foil Bearing," *Trans. ASME, J. Lubrication Tech.*, pp. 92–97.
9. Brewen, A. T., 2002, personal communication.

10. Patir, N., Cheng, H. S., 1978, "An Average Flow Model for Determining Effects of Three-Dimensional Roughness on Partial Hydrodynamic Lubrication," *Trans. ASME, J. Lubrication Tech.*, Vol. 100, pp. 12–17.
11. Hamrock, B. J., 1994, *Fundamentals of Fluid Film Lubrication*, McGraw-Hill, New York, NY.
12. Rice, B. S., 2003, *Reduction in Web-to-Roller Traction as a Result of Air Lubrication*, Ph.D. thesis, University of Rochester, Rochester, NY.
13. Jones, D. P., 1992, "Air Entrainment as a Mechanism for Low Traction on Rollers and Poor Stacking of Polyester Film Reels, and its Reduction," *ASME Special Pub. Web Handling 1992*, No. AMD-149, pp. 123–131.
14. Blok, H., vanRossum, J. J., 1953, "The Foil Bearing a New Departure in Hydrodynamic Lubrication," *Lubrication Eng.*, Dec. 1953, pp. 316–320.
15. Oberg, E., Jones, F. D., Horton, H. L., 1980, *Machinery's Handbook 23rd Edition*, Industrial Press, New York, NY.
16. Lioy, D. C., Hurtubis, E. F., Schickler, E. R., 1990, "Shot Blasted Web Conveying Roller," US Patent, 4,970,768.
17. Daly, D. A., Patterson, H. R., 1968, "Paper Guide and Drive Roll Assemblies," US Patent, 3,405,855.
18. Gross, W. A., 1980, *Fluid Film Lubrication*, John Wiley & Sons, New York, NY.